JGP Journal of General Physiology

ARTICLE

Projections from ventral hippocampus to nucleus accumbens' cholinergic neurons are altered in depression

Lucian Medrihan[1], Margarete G. Knudsen[1], Tatiana Ferraro[1], Pedro Del Cioppo Vasques[1], Yevgeniy Romin[2], Sho Fujisawa[2], Paul Greengard[1], and Ana Milosevic[1,3]

The cholinergic interneurons (ChIs) of the nucleus accumbens (NAc) have a critical role in the activity of this region, specifically in the context of major depressive disorder. To understand the circuitry regulating this behavior, we sought to determine the areas that directly project to these interneurons by utilizing the monosynaptic cell-specific tracing technique. Mapping showed monosynaptic projections that are exclusive to NAc ChIs. To determine if some of these projections are altered in a depression mouse model, we used mice that do not express the calcium-binding protein p11 specifically in ChIs (ChAT-p11 cKO) and display a depressive-like phenotype. Our data demonstrated that while the overall projection areas remain similar between wild type and ChAT-p11 cKO mice, the number of projections from the ventral hippocampus (vHIP) is significantly reduced in the ChAT-p11 cKO mice. Furthermore, using optogenetics and electrophysiology we showed that glutamatergic projections from vHIP to NAc ChIs are severely altered in mutant mice. These results show that specific alterations in the circuitry of the accumbal ChIs could play an important role in the regulation of depressive-like behavior, reward-seeking behavior in addictions, or psychiatric symptoms in neurodegenerative diseases.

Introduction

The nucleus accumbens (NAc) is a large nucleus at the ventral part of the striatum where signals from a wide variety of sensory and motor inputs converge. The NAc functions as a funnel through which information must pass and where it is finely modulated (Zahm and Brog, 1992; O'Donnell et al., 1997). The NAc circuitry is centrally involved in the assessment of reward. It selects and reinforces the behaviors that lead to a positive outcome and abandons or modifies those that result in non-productive activities, and thus has a major role in the generation of motivated behaviors (Zahm, 2000; Meredith et al., 2008). The disrupted functioning of this network has been linked to the incapacity of experiencing pleasure (anhedonia), as seen, for example, in depression (Price and Drevets, 2010; Russo and Nestler, 2013). Thus, mapping complex NAc neuronal networks with other brain regions would be fundamental for understanding the behavioral changes in mood disorders and other neurological diseases. NAc connectivity was examined using the morphological and electrophysiological approaches, as well as non-selective anterograde and retrograde tracers (Thompson and Swanson, 2010; Britt et al., 2012; Bagot et al., 2015; Christoffel et al., 2015; LeGates et al., 2018). These classical studies showed that the main brain areas that project to the NAc are the prefrontal cortex (PFC), ventral hippocampal subiculum (vHIP/Sub), basolateral amygdala (BLA), ventral tegmental area (VTA), and thalamic nuclei (Smith et al., 2004; Sesack and Grace, 2010). These areas reciprocally interact through excitatory glutamatergic inputs of the cortico-striato-pallidal-thalamo-cortical loop and by the dopaminergic projections from the VTA and substantia nigra (SN) in the mesolimbic dopaminergic pathway. Although the connections of the NAc have been well characterized, the direct cell–cell interaction with other brain areas is still not well understood. Studies showed that many diseases, major depressive disorder among them, have a strong cell- and region-specific component (Warner-Schmidt et al., 2012), making it necessary to decipher the cell type–specific circuitry between the key brain regions. The gross anatomy of inputs to numerous brain areas has been studied using traditional tracers (Gerfen and Sawchenko, 1984;

[1]Laboratory of Molecular and Cellular Neuroscience, The Rockefeller University, New York, NY, USA; [2]Molecular Cytology Core Facility, Memorial Sloan Kettering Cancer Center, New York, NY, USA; [3]Laboratory of Developmental Genetics, The Rockefeller University, New York, NY, USA.

P. Greengard died on April 13, 2019. Correspondence to Ana Milosevic: amilosevic@rockefeller.edu

L. Medrihan's current affiliation is Neuroendocrine Biosciences, Inc., San Diego, CA, USA. M.G. Knudsen's current affiliation is General Surgery, South Shore University Hospitals, Bay Shore, NY, USA. T. Ferraro's current affiliation is Drexel Medical School, Philadelphia, PA, USA. P. Del Cioppo Vasques's current affiliation is Mayo Medical School, Rochester, MN, USA. S. Fujisawa's current affiliation is ZEISS Research Microscopy Solutions, Carl Zeiss Microscopy, LLC, White Plains, NY, USA.

Bolam et al., 2000; Thompson and Swanson, 2010), but these techniques cannot distinguish connectivity to specific cell types. This has become achievable with the advent of techniques that allow cell-specific connectivity mapping (Wall et al., 2010), enabling the study of the processes in only one cell type without dissecting it out from its natural surroundings, preserving all the connections and processes that exist in vivo. Monosynaptic circuit tracing with the CRE-dependent modified rabies virus, developed by the Callaway laboratory (Wall et al., 2010) and modified by the Uchida laboratory (Watabe-Uchida et al., 2012), circumvent this limitation by using mouse lines that express CRE in a cell-specific manner. With the introduction of this cell-based approach for mapping connectivity inputs to different cell types in the dorsal striatum, including dopaminergic receptor 1 and 2 medium spiny neurons (MSNs) (Wall et al., 2013), and cholinergic interneurons (ChIs) (Guo et al., 2015; Klug et al., 2018) were elucidated. However, the cell-specific inputs to the ventral striatum have not been studied.

Striatal ChIs are giant aspiny interneurons that represent only about 0.3% of all striatal neurons (Rymar et al., 2004). Despite their under-representation, the tonically active ChIs have dominant modulating control over inputs and outputs of the main population of neurons in NAc, the medium spiny neurons (Russo and Nestler, 2013; Virk et al., 2016). Indeed, optogenetical inhibition of ChIs in the NAc increased medium spiny neurons activity and blocked the rewarding effects of cocaine (Witten et al., 2010). Chemogenetic and optogenetic manipulation of NAc ChIs interneuron activity opposed the motivating influence of appetitive cues, further emphasizing their importance for cue-motivated behaviors (Collins et al., 2019). These cells have been also shown to have a critical role in regulating depressive-like behaviors in mice (Alexander et al., 2010; Warner-Schmidt et al., 2012; Cheng et al., 2019). One of the molecular mechanisms of depressive-like behaviors is the alterations in expression levels of the calcium-binding protein S100a10 (also called p11), shown by our laboratory and others (Svenningsson et al., 2006; Zhang et al., 2011; Hanada et al., 2018; Cheng et al., 2019). Mice with a complete lack of p11 exhibit anhedonia and despair, but this depressive-like behavior can be reiterated with the region-specific knock down in NAc (Alexander et al., 2010), and specifically in the NAc ChIs (Warner-Schmidt et al., 2012; Hanada et al., 2018). Notably, this behavior appears to be governed specifically by the NAc and not caudate putamen/dorsal striatum (CPu) ChIs, since selective p11 knock down in CPu ChIs did not reproduce the depressive phenotype.

For all these reasons, it is important to examine the connectivity of these neurons to gain a better understanding of cell-specific circuitries regulating normal and pathologic behavioral outcomes. Here, we utilized the CRE-dependent monosynaptic modified rabies virus method and mapped all the brain regions and cells with direct inputs to NAc ChIs. We corroborated known areas with direct inputs to NAC but also found areas that project only to NAc but not the CPu ChIs. To trace the direct inputs to ChIs in the context of depression, we used ChAT-CRE mice with the depressive phenotype (ChAT-p11 cKO). We found that in ChAT-p11 cKO mice a significantly lower number of pyramidal cells from the ventral hippocampus (vHIP) projects to the NAc ChIs. Together, these data demonstrate the inputs to ChI neurons from a large number of discrete areas scattered throughout the brain and provide a possible mechanism of how accumbal ChI circuitry regulates depression and other NAc-related behaviors.

Materials and methods

Animals and reagents

Adult ChAT-CRE (GM60) mice obtained from GENSAT (https://www.gensat.org; gift from Dr. Nathaniel Heintz, The Rockefeller University). We utilized cell-type–specific p11 knockout mouse line (ChAT-p11 cKO) as a model of depression by breeding the p11 floxed mice to ChAT-CRE GM60 mice, as previously described (Svenningsson et al., 2006; Warner-Schmidt et al., 2012). In addition, this mouse line was also bred to GENSAT ChAT-TRAP line (Doyle et al., 2008). Additionally, the Cux2-CRE line was used (kindly donated by Ulrich Muller, Johns Hopkins School of Medicine, Baltimore, MD, USA). Camk2a-CRE line was obtained from the Jackson laboratory (B6.Cg-Tg(Camk2a-cre)T29-1Stl/J). The mouse lines were maintained in a C57BL/6 background. Mice were kept at the 12-h light/dark cycle and water and food ad libitum at The Rockefeller University animal facility. Mice of both sexes were selected for experiments when they were 8- to 16-wk old, and the selection for each experiment and mouse line was randomized. All procedures were approved by the institutional IACUC and adhere to the ARRIVE guidelines.

Viruses

Adenoviral vectors AAV2.CMV.PI.Cre.rBG and AAV2.CMV.-HI.GFP-Cre.SV40 adenoviral vectors (Watabe-Uchida et al., 2012) were purchased from the University of North Carolina at Chapel Hill Vector Core. Rabies virus vectors EnvA G-deleted Rabies-GFP or EnvA G-deleted Rabies-mCherry (Wall et al., 2010) were purchased from the GT3 Core Facility at Salk Institute.

Stereotaxic injections

We performed three types of injection: helper virus was injected into NAc, followed by the injection of the rabies virus at a different angle to avoid infection and replication of the virus in the dorsal striatum. Stereotaxic surgeries were performed under general ketamine–xylazine anesthesia. Mice were placed in the stereotaxic apparatus and injection was guided by the AngleTwo program. Coordinates for the NAc injection were +1.10 mm mediolateral, +1.80 mm anteroposterior, and −4.60 mm dorsoventral from bregma, with the head tilt of 3–5°. Coordinates for CPu injections were +1.80 mm lateral, 0.70 anterior, and −3.50 mm dorsoventral from the bregma. Each mouse was injected with 0.3–1 µl of the viral suspension using the 10-µl Hamilton syringe and 33-g Hamilton needle over 10 min and an infusion pump (World Precision Instruments). Two consecutive injections were performed on each mouse. The helper virus mixture, consisting of an equal volume of AAV1.EF1-Flex-TVA-Cherry.ape (titer 4×10^{12} vg/ml) and AAV1 CA-Flex-RG (titer 3×10^{12} vg/ml) adenoviral vectors (Watabe-Uchida et al., 2012) (University of North Carolina at Chapel Hill Vector Core),

was injected at the volume of 0.8 µl, followed by the 0.3 µl of the EnvA G-deleted Rabies-GFP (titer 1.54 × 10^9 tu/ml) or EnvA G-deleted Rabies-mCherry (titer 1.58 × 10^9 tu/ml) (Wall et al., 2010) (GT3 Core Facility at Salk Institute) 4–5 wk after the first injection. The titer of the viruses was 0.9–1 cfu ×10^6. For the injections into NAc, the second injections were performed at the 25° angle to avoid infecting the cells in the CPu with the rabies viral vector. Mice were euthanized and analyzed 1 wk after the rabies virus injection. Since this technique involves stereotaxic injection into the ventral part of the striatum, there is a possibility of unintended infection of the ChIs in the dorsal striatum along the injection route. Thus, two sets of injections were done: one into NAc and one into the dorsal striatum right above the NAc injection with the smaller (0.3 µl) and larger (0.8 µl) volume of the rabies virus. The analysis with the larger volume was used for the scanning of the whole brain for the representative images because it enables easier visualization of the projection sites.

Tissue processing and immunocytochemistry

1 wk after the injection of the EnvA G-deleted Rabies viral vector, animals were deeply anesthetized with Nembutal and intracardially perfused with 4% paraformaldehyde solution and cryopreserved through a series of sucrose dilutions. Brains were cryopreserved in a series of sucrose solutions in 0.01 M PBS and embedded in the embedding media (Tissue-Tek). A series of 30-µm–thick coronal sections throughout the whole brain were sectioned on the cryostat. Immunocytochemistry was performed as described before (Milosevic et al., 2017). In short, cryostat sections were incubated with the solution of 5% normal goat serum in PBS for 1 h, followed by overnight incubation with the primary antibodies and appropriate Alexa Fluor (Invitrogen) secondary antibodies. Primary antibodies used were anti-GFP (1/500, raised in chicken, cat#ab13970; Abcam) and mCherry (1/500, raised in rabbit, cat#167453; Abcam). Sections were coverslipped with a ProLong mounting solution.

Imaging and quantification

Imaging was performed in two ways. For representative images of the brain areas, tissue sections were first labeled with the anti-GFP or anti-mCherry antibodies, depending on the type of RV injected. Then, images were selected based on the quality of expression and imaged at the confocal microscope (LSM710 and LSM900; Zeiss). Images were taken with 10×, 20×, and two oil objectives, 40× and 63×, with the fluorescence-free immersion oil Immersol 518 (Zeiss) at room temperature. Images shown throughout the paper were processed in ImageJ (for the scale bars) and Photoshop. In Photoshop, regions with labeled cells were enlarged to enable a better visual representation of projecting neurons. Images were modified only with the brightness and contrast of Photoshop's image modification tool. Schematic diagrams were created with https://Biorender.com.

For quantification, three biological and technical replicate samples were used for control and ChAT-p11 cKO. Imaging for quantification was performed on a series of sections, immunolabeled with anti-GFP or anti-mCherry antibodies, and counterstained with DAPI to better delineate histological layers and anatomical structures. Sections that were used for quantification represented every other 30-µm–thick section throughout the whole brain. Imaging was performed with the Mirax Scan scanning system (Zeiss). The resulting low magnification images represented 5 × 5 tiled images of a whole brain section. These images were loaded into the Panoramic-View software and areas with GFP-labeled cells were outlined in their respective brain regions. The expression sites delineations were made in accordance with The Mouse Brain atlas (Franklin and Paxinos, 2008) and Scalable Brain Atlas (http://scalablebrainatlas.incf.org/) as reference. MetaMorph Image Analysis software was used for the automatic quantification of GFP- or mCherry-labeled cell bodies in each region, and ImageJ/Fiji (Schindelin et al., 2012) was used for the semiautomatic conformation of the cell body numbers. Differential enrichment of cell bodies between different regions and respective graph bar charts was completed using the Prism software. For this analysis, only areas that appear in at least two samples were analyzed. Areas at the injection sites, as well as septal, basal forebrain, extended amygdala, and cortical–amygdala transitory areas that contain a large number of ChI neurons were not included in the analysis. We used Paxinos atlas to outline the brain regions, and the abbreviations for these regions are shown in Table 1.

Optogenetics

Mice were anesthetized with a ketamine/xylazine cocktail and underwent stereotaxic surgery to inject serotype 5 adeno-associated viruses (AAV) encoding CaMK2a-ChR2 (H134R) (AAV5/CaMKII-hChR2(H134R)-eYFP-WPRE, titer 6 × 10^{12} vg/ml; UNC Viral Vector Core), and control virus rAAV5/CaMKII-EFYP (titer 4.3 × 10^{12} vg/ml; UNC Viral Vector Core). The virus was injected bilaterally into the vHIP (from bregma: anterior/posterior: −3.8, lateral: +3.0, dorsal/ventral: 4.5 from top of skull) at a rate of 0.1 ml per minute for 10 min. Mice recovered for 5–6 wk before being subjected to electrophysiological experiments. For electrophysiological recordings, field light stimulation of ChR2-expressing vHIP terminals in NAc neurons was done through a 40× objective using a SPECTRA X LED light engine (Lumencor).

Electrophysiology

Mice between 8 and 12 wk of age were euthanized with CO_2. Coronal slices (300 µm thickness) were cut using a Vibratome 1000 Plus (Leica Microsystems) at 2°C in a NMDG-containing cutting solution (in mM): 105 NMDG (N-Methyl-D-glucamine), 105 HCl, 2.5 KCl, 1.2 $NaH2PO_4$, 26 $NaHCO_3$, 25 glucose, 10 $MgSO_4$, 0.5 $CaCl_2$, 5 L-ascorbic acid, 3 sodium pyruvate, 2 thiourea (pH was around 7.4, with osmolarity of 295–305 mOsm). After cutting, slices recovered for 15 min in the same cutting solution at 35°C and for 1 h at room temperature (RT) in aCSF recording solution containing (in mM): 125 NaCl, 25 $NaHCO_3$, 2.5 KCl, 1.25 $NaH2PO_4$, 2 $CaCl_2$, 1 $MgCl_2$, and 25 glucose (bubbled with 95% O_2 and 5% CO_2) (see below). Whole-cell patch-clamp recordings were performed with a Multiclamp 700B/Digidata1550A system (Molecular Devices), an upright Olympus BX51WI microscope equipped with the appropriate filters (Olympus) and a SPECTRA X LED light engine (Lumencor). The

Table 1. **List of anatomical structure abbreviations used in the study**

Region	Subregion
Cortex	FrA - frontal association
	InCx – insular
	LO - lateral orbital
	MO - medial orbital
	VO - ventral orbital
	PrL - prelimbic
	Cg - cingulate
	M - motor
	S - somatosensory
	Au - auditory
	V - visual
	Cl & DEn – claustrum & dorsal endopiriform nucleus
	Ent – entorhinal
	PRh - perirhinal
	Pt Cx – parietal associative
Hippocampus	ventral - vHIP
	CA1-2 field CA1 and CA2 hippocampus
	Sub - subiculum
Striatum	CPU-caudate putamen, dorsal striatum
	NAc - nucleus accumbens, ventral striatum
Amygdala	BLA-basolateral amygdaloid nucleus
	BMP-basomedial amygdaloid nucleus
	CeN – central amygdaloid nucleus
	MeA – medial amygdaloid nucleus
	AA – anterior amygdaloid nucleus
Thalamus	AD - anterodorsal nucleus
	AM – anteromedial nucleus
	AV – anteroventral nucleus
	CL – centrolateral nucleus
	CM – central medial nucleus
	VM – ventromedial nucleus
	MD – mediodorsal nucleus
	IAD – interanterodorsal nucleus
	IAM – interanteromedial nucleus
	IMD - intermediodorsal thalamic nucleus
	IMD - intermediodorsal thalamic nucleus
	PF - parafascicular nucleus
	PC – paracentral nucleus
	PV – paraventricular thalamic nucleus
	PT - paratenial thalamic nucleus
	VA – ventral anterior
	lat THA – lateral thalamus
	med THA – medial thalamus
Subthalamus	PSTh - parasubthalamic nucleus
	ZI – zona inserta
Hypothalamus	LH-lateral hypothalamus
	Pa - paraventricular hypothalamic nucleus
	Pe – periventricular hypothalamic nucleus
	PH – posterior hypothalamic nucleus
	MP medial preoptic nucleus
	VMH – ventromedial hypothalamic nucleus
Brainsteam: Midbrain, pons & medulla	SNc/SNr - substantia nigra, compacta, reticulata
	VTA-PBP- ventral tegmental are parabrachial nucl.
	DR- dorsal raphe
	PR – prerubral field
	RN-red nucleus
	PTg-pedunculopontine tegmental nucleus
	PAG periaqueductal gray
	Re - reunions
	RRF - retrorubral field
	LPB – lateral parabrachial nucleus
	MBP-medial parabrachial nucleus
	LC-locus coeruleus

slice was placed in a recording chamber (RC-27L; Warner Instruments) and constantly perfused with oxygenated aCSF at 24°C (TC-324B; Warner Instruments) at a rate of 1.5–2.0 ml/min. The intracellular solution contained (in mM): 126 K-gluconate, 4 NaCl, 1 $MgSO_4$, 0.02 $CaCl_2$, 0.1 BAPTA, 15 glucose, 5 HEPES, 3 ATP, 0.1 GTP (pH 7.3). We used a whole-cell current-clamp for electrophysiology recordings in layer II/III PFC neurons. For measuring the membrane potential, 30 s of recording were binned into 0.5 ms bins and fitted with a Gaussian. For measuring the action potential firing, small currents were injected into the cells to bring the membrane potential to −70 mV. Consecutive 1-s current steps of 50 pA starting from −100 pA were injected to induce depolarization. The action potential threshold was measured from the first action potential to avoid any confounding effects of adaptation. For electrophysiology recording in NAc, we used whole-cell current-clamp to record the tonic activity of ChI neurons.

Consecutively, we used whole-cell voltage-clamp configuration to record evoked glutamatergic responses in ChI or medium spiny neurons. For this, we used field light stimulation of ChR2-expressing vHIP terminals in NAc in the presence of 30 µM bicuculine (to block GABAergic transmission). Consecutively, we used whole-cell voltage-clamp configuration to record evoked synaptic responses in ChIs or medium spiny neurons. For this, we used field light stimulation of ChR2-expressing vHIP

terminals in NAc in the presence of 30 μM bicuculine (to block GABAergic transmission). The photostimulation-induced currents were blocked completely by the subsequent addition of glutamate receptor antagonists AMPA (DNQX 20 μm) and NMDA (APV 50 μm) receptor antagonists.

Online supplemental material

Fig. S1 contains images of the different brain regions that contained GFP- or mCherry-labeled cells, representing neurons projecting to the NAc and CPu ChIs.

Results

We sought to determine direct inputs onto the ChI neurons of the NAc using the monosynaptic circuit tracing method with the CRE-dependent modified rabies virus technique (Wall et al., 2010; Watabe-Uchida et al., 2012). This method utilizes the spread of rabies virus (RV) through the synapses onto the projecting neurons. However, this spread is limited to the direct, primary input onto the infected cells due to several modifications in the rabies virus genome. We used the previously characterized ChAT-CRE mouse line GM60 (https://www.gensat.org). The experimental design was adapted to allow the optimal infection of the sparce cell population. ChI neurons were labeled with stereotaxic injection of a mixture of two viruses, one carrying the G-protein and another carrying the TVA receptor. This was followed by injection of a rabies virus into the same NAc region 5 wk later (Fig. 1, A and B). We confirmed that helper viruses, carrying the mCherry tag, infected ChI neurons by immunocytochemical labeling with anti-mCherry and anti-ChAT antibodies (Fig. 1 C). Next, we confirmed that viral injections infected only NAc ChI neurons using the mouse line ChAT-CRE crossed to ChAT-TRAP (https://www.gensat.org) in which all ChI neurons are tagged with the GFP (Doyle et al., 2008). We immunolabeled a series of coronal sections with an anti-mCherry antibody and detected no $mCherry^+$ GFP^+ cells in the neighboring brain regions with ChI neurons (Fig. 1 D). Furthermore, because the injection into NAc infects the dorsal striatum–caudate putamen ChI cells along the needle track, a set of control injections into the CPu was performed to determine the overlap with the CPu ChIs projections.

To generate a comprehensive list of all projection sites and to quantify the number of neurons that project to NAc ChIs, we analyzed the whole brain, as described in detail in the Materials and methods section. The cells retrogradely labeled with RV-GFP virus were detected in distinctive subregions of the cortex, hippocampus, thalamus, hypothalamus, amygdala, and brainstem (Fig. 2 and Fig. S1 A). The representative images of the NAc ChAT projection sites are shown in Fig. 2, A–G, while a complete list of all regions and proportions of labeled cells in each area is shown in Fig. 2 H. In addition, to gain insight into the similarities and differences between the NAc and CPu projections, we also analyzed the brains injected into the CPu (Fig. S1 B). Notably, the regional distribution of cells labeled with the rabies virus after the CPu and NAc injections had some very distinct areas with labeled cells (Fig. S1, A and B). This suggested that NAc ChIs have a distinct set of regions that project exclusively to these cells and not the CPu ChIs.

Cortical projections to NAc ChIs

A large proportion of labeled cells in the brains that have been injected into NAc was found in the discrete areas of the PFC (Fig. 2 H). These included medial (Fig. 2 A1) and lateral orbital cortex (Fig. 1 A1), agranular insular cortex, prelimbic cortex (Fig. 2 A2), and anterior cingulate cortex (Fig. 2 A3). The majority of the projections came from the ipsilateral side (Fig. S1 A), as opposed to CPu where a substantial projection from the contralateral side was reported (Schmidt et al., 2012).

In the orbital areas of the PFC, in the NAc-injected brains, large number of labeled cells were found in the medial and ventral orbital (MO-VO) region of the PFC, while they were absent in the CPu-injected brains (Fig. 3, A1 and A2). Prefrontal cortical areas contained a large number of labeled neurons in layer 2/3 (Fig. 2, A1 and A2; and Fig. 3 A1). This is the opposite of what was found after CPu injection, where labeled cells were concentrated in the deep cortical layers (Fig. 3 A2 and [Guo et al., 2015; Klug et al., 2018]). To confirm that layer 2/3 cells in MO-VO were indeed glutamatergic pyramidal cells that project to NAc ChIs, two sets of experiments were performed. First, we adapted the injection approach to test the connectivity. For this purpose, we used another mouse line with a CRE expression under the regulation of the Cux2, a specific marker for layer 2/3 pyramidal neurons (Franco et al., 2012). Helper virus, tagged with mCherry, was injected into the upper layers of the MO-VO cortex of the Cux2-CRE mouse line (gift from Ulrich Muller, Johns Hopkins School of Medicine), followed by the injection of the RV-GFP into the NAc 5 wk later, as shown in the schematic diagram in Fig. 3 B. This injection approach enabled layer 2/3 projecting neurons to be infected with the helper virus via axonal ends in the NAc. The consecutive RV-GFP injection and recombination enabled projecting neurons labeled with the helper virus to express the GFP. The resulting double-labeled cells (mCherry/GFP) in the medial orbital cortex layer 2/3 are shown in Fig. 3 C. Second, a set of electrophysiological recordings were done to confirm our initial data (Fig. 3, D–H). We used a whole-cell patch clamp to record from layer 2/3 neurons infected with RV-GFP and the helper virus, respectively. The firing frequency, as well as the membrane potential and action potential threshold of the recorded neurons, were characteristic of pyramidal neurons (Fig. 3 D) and were not changed between neurons infected with the different viruses (Fig. 3, E–H). These experiments confirmed that layer 2/3 in the MO-VO are indeed pyramidal projecting neurons and that their basic physiological properties are not altered by the virus injection protocol. Interestingly, Wfs1-expressing cells with the same layer and regional specificity project to the motor cortex and CPu and receive projections from the lateral amygdala, posterior thalamic group, and several cortical areas (Shrestha et al., 2015), suggesting that multiple subtypes of the layer 2/3 neurons from the medial orbital cortex project outside of the cortex.

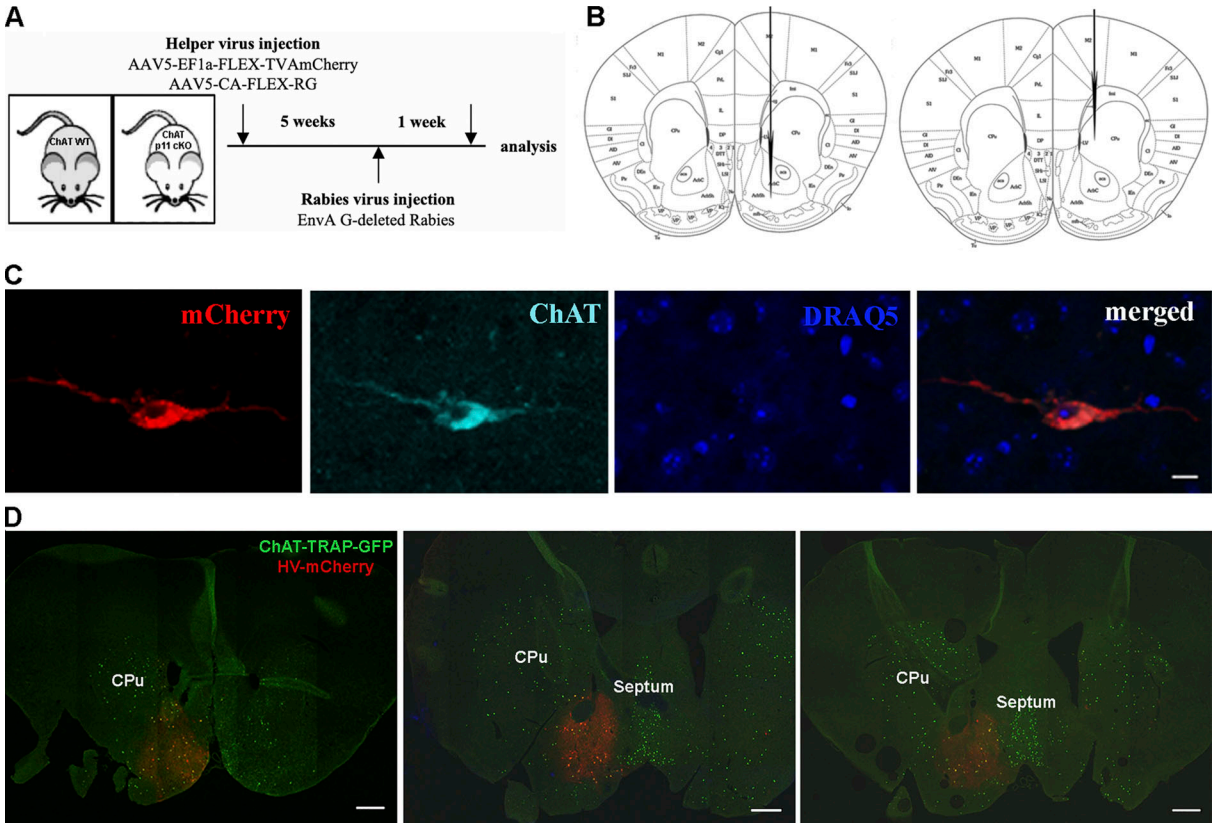

Figure 1. **ChI cells in NAc are successfully infected utilizing the rabies monosynaptic tracing method. (A)** Injection schedule and types of viruses used for axonal tracing. **(B)** Schematic diagram showing the areas of the brain injected with the viruses. **(C)** Representative image of the cell in the NAc infected with the mixture of helper viruses (red, mCherry) and immunolabeled with the anti-ChI antibody. Scale bar, 10 µm. **(D)** Series of low magnification images of the sagittal sections of the mouse line ChAT-CRE crossed with the ChI-L10a-EGFP injected with the helper (mCherry) virus into the NAc. Sections were labeled with the mCherry (red) and GFP (green) antibodies to enable visualization of the infection efficacy in the ChI cells. The majority of infected cells, double-labeled with mCherry and GFP (yellow) are found in the NAc, with no major infection of the ChIs in the adjacent areas of the dorsal striatum, basal forebrain, and septum. Distance from the bregma: ∼1.54 mm (left image); ∼0.74 mm (middle image); ∼0.38 mm. Scale bars, 500 µm.

ChI circuitry is changed in a depressive-like mouse model

To better understand the circuitry at the root of depressive behavior, we investigated projections between control and depressive-like mouse model ChAT-p11 cKO mice. Quantitative analysis was performed on four brain regions: MO-VO, amygdala, vHIP, and dorsal raphe. These areas were selected because they have been shown to have an important role in depressive-like behaviors (Price and Drevets, 2010; Stuber et al., 2011; Chaudhury et al., 2015; Hultman et al., 2018) and because MO-VO, amygdala, and vHIP project specifically to the NAc ChIs. Representative images of projections from MO-VO, vHIP, and dorsal raphe used for this quantification are shown in Fig. 4 A. Quantification of projections has shown a significantly larger number of projections from vHIP in the ChAT-CRE control (CTR) mice than in ChAT-p11 cKO (Fig. 4 B). A significant difference was not reached for MO-VO, amygdala, and dorsal raphe, although there is a trend toward a lower number of projections from the amygdala and higher number of projections from MO-VO in ChAT-p11 cKO.

Virtually, all labeled cells in the hippocampus were confined to the ventral part, namely subiculum and CA1 (Fig. 2 F; Fig. 4 A; and Fig. S1, A4 and A5). No direct input to the CPu ChIs was detected. This corroborated and expanded on previous findings that the ventral subiculum has a strong projection to NAc (Britt et al., 2012; Bagot et al., 2015; LeGates et al., 2018). To verify if the connections from vHIP to the NAc ChI neurons are functionally altered by the p11 deletion, we expressed channelrhodopsin (ChR) in vHIP pyramidal neurons (Fig. 4, C and D) of the Ca^{2+}/calmodulin-dependent protein kinase (Camk2a)-CRE mouse that specifically label projection neurons because Camk2a promoter has been traditionally used as an excitatory neuron-specific promoter (Basu et al., 2008; Tye et al., 2011). First, we confirmed that optically evoked currents are blocked completely by glutamate receptor antagonists (CNQX/AP5), and we amended the Materials and methods section to show that. We have shown before that deletion of p11 from ChI neurons results in a decrease in their firing frequency (Cheng et al., 2019), so we used this to identify the ChI neurons by their tonic firing in acute slices containing NAc from CTR and p11 KO mice (Fig. 4 E). Next, we recorded photostimulation-evoked glutamatergic currents of the vHIP terminals in NAc ChI neurons from CTR and p11 KO mice. In the CA1 area of the hippocampus, it is highly expressed exclusively in pyramidal neurons (Wang et al., 2013), and the direct glutamatergic projection between the pyramidal neurons in vHIP and medium spiny neurons in NAc has been previously described (Bagot et al., 2015; Muir et al., 2020). We

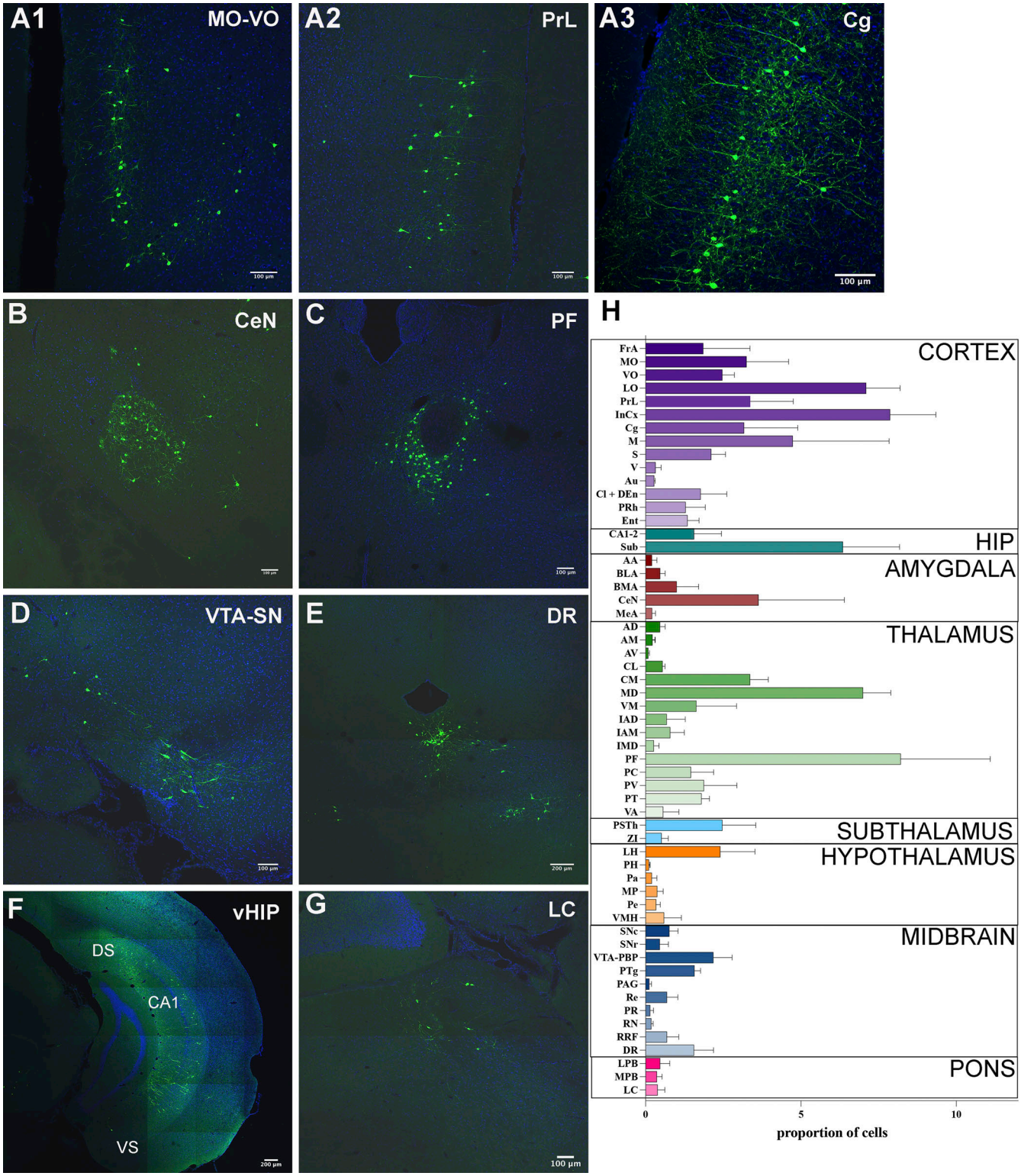

Figure 2. **Representative images of the brain areas that project directly to the NAc ChIs and are implicated in depressive-like phenotype based on the literature. (A–G)** Anti-GFP antibody immunolabeling revealed cells in several cortical areas including medial (MO) and ventral orbital (VO) prefrontal areas shown in A1, prelimbic cortex (PrL) in A2 and cingulate cortex (Cg) in A3; (B) central amygdaloid nucleus (CeN), (C) parafascicular thalamic nucleus (PF), (D) ventral tegmental area and substantia nigra (VTA-SN), (E) dorsal raphe (DR), (F) ventral hippocampus (vHIP), with large number of GFP$^+$ cells in CA1 region, dorsal subiculum (DS) and ventral subiculum (VS); and (G) locus coeruleus (LC). **(H)** Graph represents the proportion of RV-GFP infected cells quantified throughout the brain of mice injected in the NAc. Graph bars are represented as the mean of the total number of cells in each region ± SEM from three replicate samples. Distance from the bregma: (A1) ~2.58 mm, (A2) ~1.94 mm, (A3) ~1.10 mm, (B) approximately −1.34 mm, (C) approximately −2.18 mm, (D) approximately −2.92 mm, (E) approximately −4.60 mm, (F) approximately −3.80 mm, (G) approximately −5.40 mm. HIP - hippocampus.

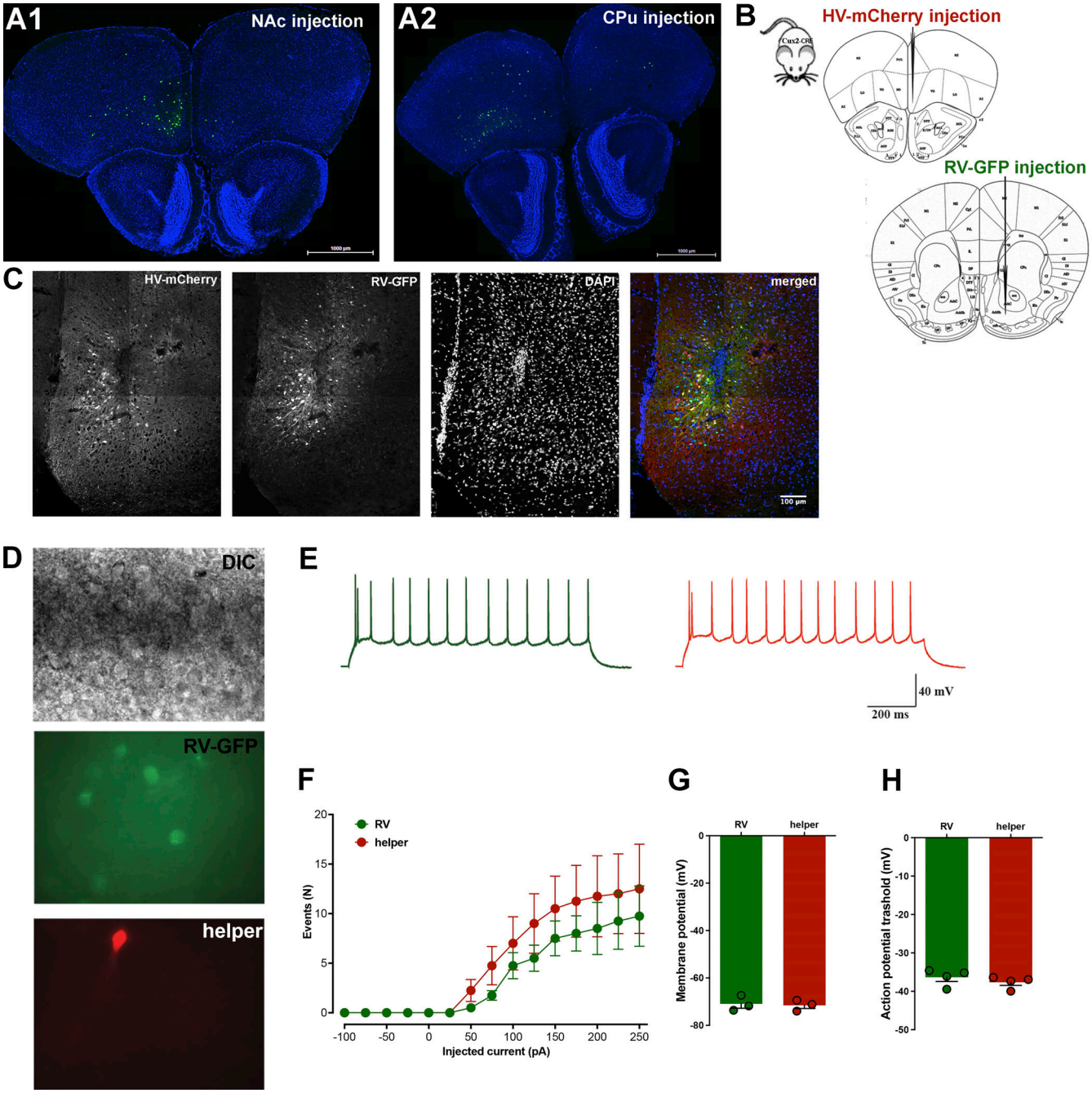

Figure 3. **Layer 2/3 pyramidal neurons from the prefrontal cortical areas project to NAc ChIs. (A1 and A2)** Low-magnification images from the prefrontal cortex MO-VO showing layer 2/3 neurons (A1) in contrast to layer five neurons that project to CPu ChIs (A2). **(B)** Experimental design of injections into the Cux2-CRE mouse line to label the medial orbital cortex MO layer 2/3 neurons that project to NAc ChIs. Mouse was first injected with the helper virus (mCherry) into the MO, followed by injection of RV-GFP into the NAc. **(C)** Immunocytochemistry of the MO cortex of the Camk2a-CRE mouse labeled the anti-mCherry and anti-GFP antibodies, showing that some cells infected with the helper virus ($mCherry^+$) and rabies virus (GFP^+) are double-labeled ($mCherry^+$ GFP^+, merged). **(D)** Representative cells in the layer 2/3 of the CaMK2a-CRE mouse prefrontal cortex labeled with the helper virus into the MO-VO followed by the RV-GFP injection into the NAc that were used for electrophysiology recordings. **(E)** Representative cells with traces of the firing response to a 250-pA step injection of current in layer 2/3 MO-VO pyramidal neurons infected with RV-GFP (GFP, green) and helper virus (mCherry, red). **(F)** The representative firing traces firing frequency of layer 2/3 MO-VO pyramidal neurons infected with RV-GFP (n = 4 neurons/3 mice) or helper virus (four neurons/three mice) in response to 50-pA current steps injections. **(G and H)** Histograms showing the membrane potential (F) and the voltage threshold (H) for action potential firing in layer 2/3 MO-VO pyramidal neurons infected with RV-GFP or helper virus.

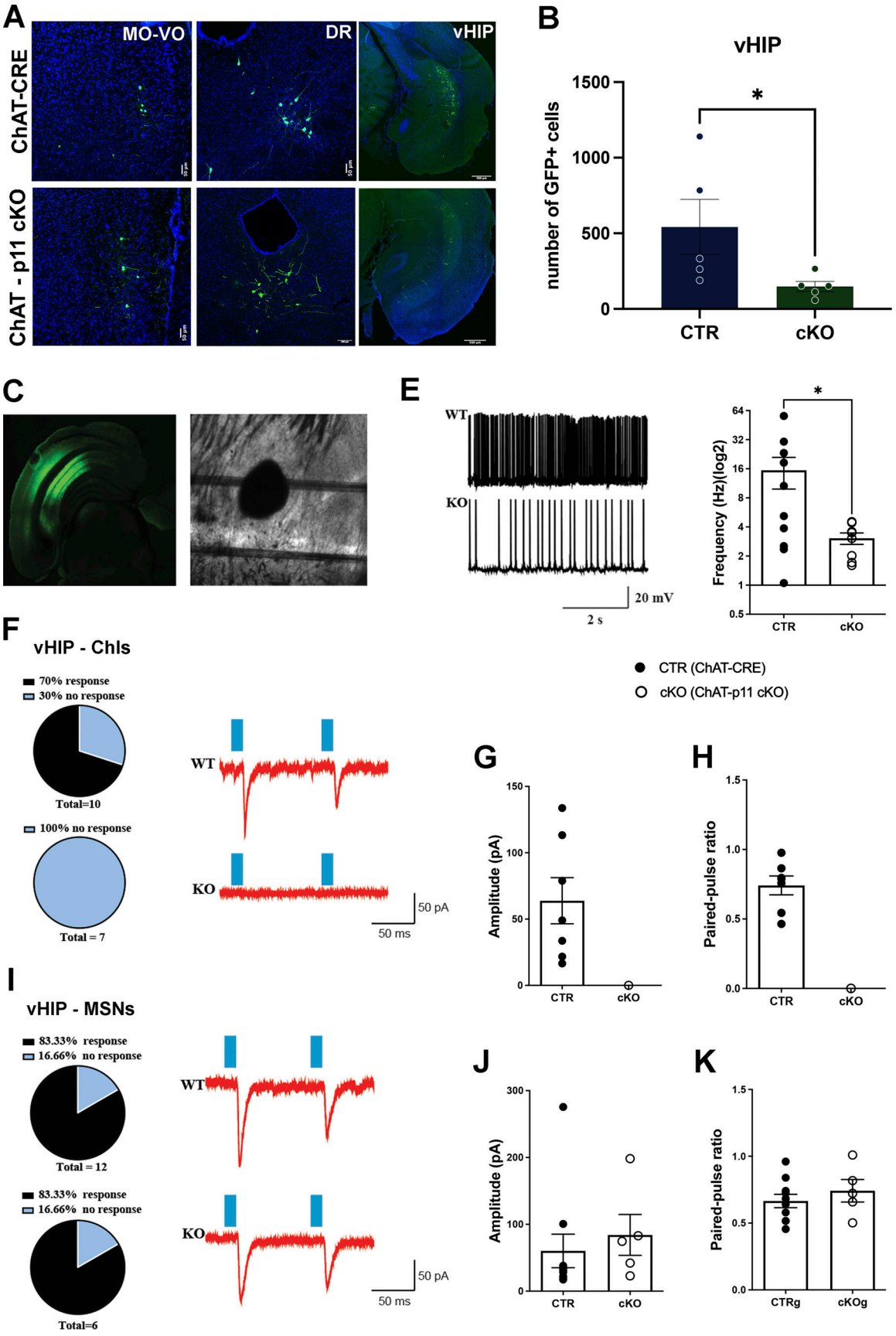

Figure 4. **Mouse model of depression—ChAT-p11 cKO shows differential projections to NAc ChIs. (A)** Representative images of projection neurons labeled with RV-GFP in MO-VO region of the prefrontal cortex, DR, and vHIP in ChAT-CRE and ChAT-p11 cKO mice lines. The injections were designed to infect

a small number of cells to allow optimal quantification of projecting neurons. **(B)** Quantification of GFP⁺ cells in MO-VO, DR, AMY, and vHIP regions showed significantly different number of cells only in vHIP region between ChAT-CRE control (333.0, *n* = 5) and ChAT-p11 cKO (152.0, *n* = 5) PVal = 0.0317; Mann–Whitney *t* test. **(C)** Low-magnification image of ventral hippocampus showing CaMK2a-ChR2 (H134R)—eYFP infection CA1 and subiculum pyramidal neurons. **(D)** Differential interference contrast image showing the area from NAc where we recorded from ChI and MSN neurons. **(E)** Representative traces of tonic firing of ChI neurons from control (CTR) and p11 KO mice and histograms quantifying the firing frequency of recorded neurons from each genotype, * PVal = 0.0499, Kolmogorov–Smirnov test (*n* = 10 neurons/4 mice for CTR and 8/3 for p11 KO). **(F)** Pie chart showings the percentage of CTR and p11KO ChI neurons that responded to ChR2 stimulation of vHIP terminals in NAc and representative paired-pulse (100 ms interstimulus) traces in response to ChR2 field light stimulation. **(G and H)** Histograms showing the amplitude of the first response (gE) and the paired-pulse ratio at 100 ms interstimulus (H) in response to ChR2 field light stimulation of NAc in CTR and p11KO ChI neurons. **(I)** Pie chart showings the percentage of CTR and p11KO MSN neurons that responded to ChR2 stimulation of vHIP terminals in NAc and representative paired-pulse (100 ms interstimulus) traces in response to ChR2 field light stimulation. **(J and K)** Histograms showing the amplitude of the first response (J) and the paired-pulse ratio at 100 ms interstimulus (K) in response to ChR2 field light stimulation of NAc in CTR and p11KO MSN neurons.

applied a paired-pulse protocol with two light pulses (1–2 ms) separated by 100-ms intervals to verify first if the connections between vHIP pyramidal neurons and NAc neurons are functional and second if the connections show normal short-term synaptic plasticity. While in the CTR ChI neurons, we were able to elicit glutamatergic postsynaptic responses in 70% of the recorded neurons, we could not find any response in p11 KO ChI neurons in multiple mice (Fig. 4, F–H). To validate our recording protocol, we took advantage of the well-established connection between medium spiny neurons (MSN) and HIP (Bagot et al., 2015; LeGates et al., 2018) by recording photostimulation-evoked glutamatergic currents in neighboring MSN neurons from the same slices. In each NAc slice in which we recorded photostimulation-evoked currents in ChI neurons, we recorded multiple neighboring MSN neurons as a control for the vHIP-NAc projection. Some of the patched MSN neurons (16.7%) did not respond to photostimulation; however, we had the same percentage of responsive MSN neurons in each slice from which we presented ChIs data in both genotypes. Thus, we are positive that the percentage of non-responsive ChI neurons is not random between genotypes and it is not due to the absence of glutamatergic input from vHIP. Using this paired-pulse protocol, we evoked glutamatergic responses in 83.3% of the tested MSN neurons in both CTR and p11 KO mice, and both the amplitude of the response and the paired-pulse ration were unchanged between the genotypes (Fig. 4, I–K). Taken together, these data show for the first time the existence of functional glutamatergic synaptic connections between vHIP pyramidal neurons and ChIs in NAc and further emphasize the alterations of these projections induced by the deletion of p11 in these neurons.

Accumbal ChIs receive inputs from many brain areas regulating complex behaviors

Large number of areas contained cells labeled by retrogradely transferred rabies virus after injections into the NAc and CPu (Fig. S1, A and B).

Labeled cells were distributed in distinct areas of the amygdala. In NAc-injected brains, central amygdaloid nucleus (CeN) prominently displayed a large number of GFP⁺ cells (Fig. 2 B and Fig. S1 A). When brains injected into the NAc and CPu were examined, labeled cells were distributed in distinct areas. In NAc-injected brains, CeN contained a vast majority of labeled cells (Fig. 2 B). We observed a very small number of GFP⁺ cells in the BLA, suggesting that these inputs synapse on other types of accumbal neurons. It is well-established that the amygdala, especially the basolateral amygdaloid nucleus project to the striatum (Stuber et al., 2011). More recently, cell-based tracing methods showed that both central and BLA project specifically to dopaminergic receptor 1 medium spiny neurons in the dorsal striatum (Wall et al., 2013). Functional studies investigating the role of amygdalar subdivisions linked BLA and CeN to fear conditioning (Haubensak et al., 2010; Tye et al., 2011) and memory consolidation (Paré, 2003), while lesions of the CeN reduced stress response and anxiety and fear response to chronic unpredictable stress (Ventura-Silva et al., 2013). In the brains injected into the CPu, labeled neurons were predominantly in the anterior cortical, central, and medial amygdaloid nuclei. Interestingly, we did not observe cells in basolateral or central amygdaloid nuclei, suggesting distinct inputs to ChI neurons from the dorsal and ventral striatum. The data presented here demonstrate strong connectivity of CeN to the NAc ChIs, and connectivity of BLA to other accumbal cells would suggest the intricate modulation of fear conditioning, anxiety, and stress responses in the striatum.

The majority of labeled cells in the thalamus of the brains injected into the NAc were concentrated in parafascicular, mediodorsal, and centromedial thalamic nuclei (Fig. 2 C; and Fig. S1, A2 and A4). It is notable that inputs to the CPu ChIs came from a different set of nuclei (Fig. S1, B2, B4, and B5; and [Guo et al., 2015; Klug et al., 2018]), with few exceptions such as parafascicular nucleus, which projects to both dorsal and ventral striatal ChIs. Others have shown that both dopaminergic receptor 1 and 2 medium spiny neurons receive afferents predominantly from parafascicular and mediodorsal nuclei, as well as a smaller number of inputs from ventromedial, anterodorsal, and anteroventral nuclei (Wall et al., 2013). This would imply that the thalamo–striatal connectivity targets both projection neurons and interneurons, bringing an additional level of complexity in control over striatal activity.

The hypothalamus of mice injected in the NAc contained a very small number of labeled cells, scattered mostly in the lateral hypothalamic area (Fig. 2 H and Fig. S1 A3). The lateral hypothalamic area has been shown to connect with basomedial and anterior cortical amygdaloid nuclei (Niu et al., 2012) and has a role in food intake regulation (Stanley et al., 2010; Pérez et al., 2011). This would suggest that inputs to ChI neurons in NAc have a role in modulating the behavior related to feeding and/or food intake.

Strong labeling of neurons in SN and VTA after NAc injection were observed (Fig. S1 A6). The striatal–VTA circuitry was implicated in the regulation of stimulus-dependent learning (Brown et al., 2012), as well as reward behavior (Chaudhury et al., 2013). The projections from SN and VTA to the neurons of the dorsal striatum cells are well documented (Wall et al., 2013; Guo et al., 2015; Klug et al., 2018). Here, we have shown for the first time that the part of this circuitry involves the SN/VTA-NAc ChI connectivity.

Dorsal raphe contained labeled cells in the brains from NAc and CPu injection. This affirmed previous findings about relatively weak serotoninergic inputs into the striatum (Waselus et al., 2006), and specifically ChI cells (Cachope et al., 2012; Guo et al., 2015; Klug et al., 2018). Interestingly, and not previously reported, we found virally labeled cells to be confined only to the ipsilateral side of the brain (Fig. 2 E).

Medulla, and specifically locus coeruleus, the main noradrenergic output in the brain contained few labeled cells. In addition, we detected very few neurons in other areas of the pons and medulla, most notably the area of the gigantocellular reticular nucleus. However, these neurons were sparse and thus difficult to be assigned to the appropriate nuclei. This is probably due to the technical limitations of the technique used in this study but may also represent the actual in vivo representation of connectivity within the brain.

Discussion

Mapping complex networks between the neurons in different regions of the central nervous system is essential to understanding the behavior and its changes in neurological diseases. Here, we have generated a detailed, exhaustive brain-wide map of direct projections to the cholinergic neurons in the NAc (Fig. 5 A). Importantly, this mapping revealed several areas that project only to the ventral but not dorsal striatal ChIs, such as layer 2/3 from the medial and ventral subdivisions of the orbital PFC, CeN, and subiculum of the vHIP. Most importantly, the circuitry between NAc ChIs and vHIP is significantly altered in the mouse model of depression, ChAT-p11 cKO (Fig. 5 B), with implications for cognizing the specific morphological and anatomical changes in psychiatric diseases involving these brain networks.

The NAc is involved in mediating an altered perception of social status (Berton et al., 2006), inability to experience pleasure and positive emotions, heighten negative emotional processing, psychomotor retardation (Epstein et al., 2006), and behaviors related to reward (Russo and Nestler, 2013), all distinctive traits of mood disorders and depression. The final output from the NAc and regulation of behavioral outcomes is determined by the ChIs activity. This is accomplished by integrating the large number of inputs from various regions and different neurotransmitter systems that allow fine coordination of ChIs tonic activity. For example, silencing the activity of NAc ChIs increases the activity of medium spiny neurons, the main output cells of the NAc (Witten et al., 2010). Based on these data, functional implications of the NAc ChIs circuit mapped in this study and its role in depressive behavior most likely depend on the projections unique to NAc, namely, MO-VO PFC areas, vHIP, and CeN. Circuits between these areas and the NAc are known for their role in a wide range of behaviors, including depressive behaviors. The complex regulation of the NAc output governed by the groups of neurons within the orbitofrontal cortex and their extensive circuitry with other brain regions has been described (Pinto and Sesack, 2000; Sesack and Grace, 2010; Hultman et al., 2018). For example, the PFC-NAC circuitry provides executive control by mediating task-switching behaviors and inhibiting motor responses (Sesack and Grace, 2010). An increase in the synchronized activity between vHIP and NAc predicted vulnerability to stress in naïve mice and was a marker for mice susceptible to social stress (Hultman et al., 2018). In this study, we reported several notable findings regarding the connectivity of this region with NAc. We found that layer 2/3 pyramidal cells project directly to the NAc ChIs. This is similar to the wolframin- and Ntf3-expressing layer 2/3 pyramidal neurons, which project to the dorsal striatum, and regulate stress-induced depressive-like behavior in mice (Shrestha et al., 2015). Furthermore, a large body of work has shown that layer 2/3 pyramidal neurons are mostly involved in intracortical circuits (Yoshimura et al., 2005; Shepherd, 2013). Our data and data from others (Thompson and Swanson, 2010; Shrestha et al., 2015) found projections from layer 2/3 to subcortical regions. This adds another layer to the cortical circuitry complexity, as the PFC is to our knowledge the only area where layer 2/3 pyramidal neurons project outside of the cortex. Also notable is the heterogeneity between layer 2/3 pyramidal cells since wolframin and Ntf3 expressing neurons do not project to the NAc, while we found neurons in the same region and layer specificity that synapse on the NAc ChIs. Furthermore, it was reported that direct inputs to CPu ChIs arise primarily from the motor areas, and much less from the PFC areas, such as lateral orbital, prelimbic, and cingulate (Guo et al., 2015; Klug et al., 2018). This may also imply that prefrontal cortical areas project more heavily to the NAc ChI neurons then hippocampal neurons or amygdala, as suggested before (Britt et al., 2012). Our data support this hypothesis and further show that the vHIP and the MO-VO cortices project directly and specifically to ventral, but not dorsal ChIs. These results point to the complex circuitry between the medial orbital cortex and striatum involved in depressive-like behaviors in mice.

However, it is also important to consider that the regulation of depressive phenotype in ChAT-p11 cKO depends mainly on the glutamatergic inputs from the vHIP, as they were shown here to be significantly reduced in these mice. The role of glutamatergic projections to the NAc in the regulation of addiction, anxiety, reward, and depressive behavior has been reported previously (Britt et al., 2012; Bagot et al., 2015; LeGates et al., 2018; Muir et al., 2020) although the specific mechanism reported differs between studies. Britt et al. suggested that ChIs and possibly other interneurons in NAc do not receive direct input from the vHIP but indirectly through connections with the medium spiny neurons (Britt et al., 2012). On the other hand,

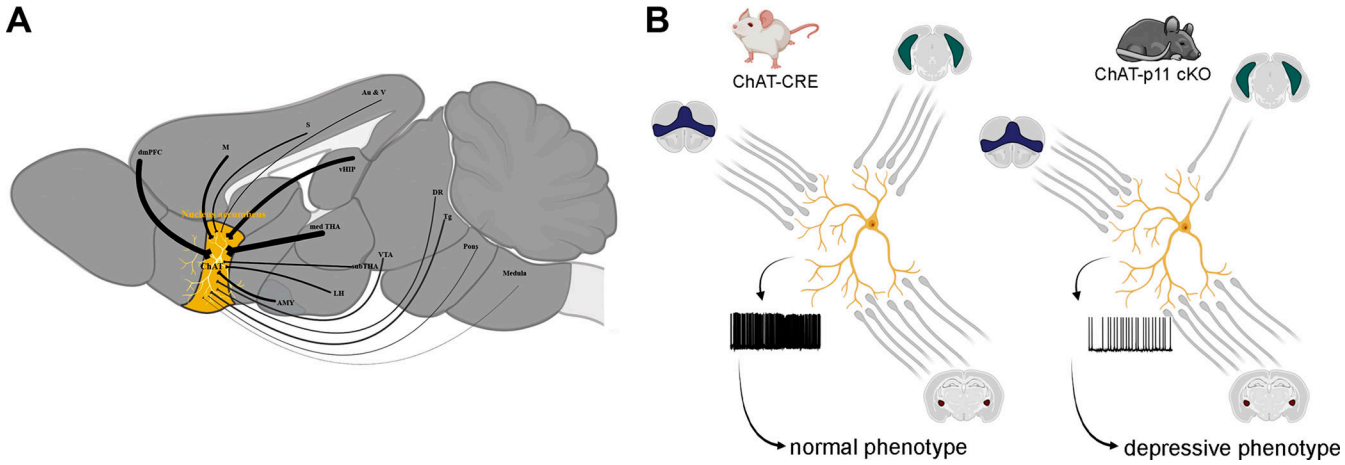

Figure 5. **Working model of the major circuitry change in the ChAT-p11 cKO mouse model of depression. (A)** Summary of the major projections to the ChIs of the nucleus accumbens: ChIs of the nucleus accumbens receive large number of projections from multiple regions of the brain. The line width represents the proportion of cells in that brain region projecting to the nucleus accumbens, relative to other regions. dmPFC – dorsomedial prefrontal cortex; M – motor cortex; S – somatosensory cortex; Au & V – auditory and visual cortices; vHIP – ventral hippocampus; medTHA - medial thalamic nuclei; LH - lateral hypothalamus, AMY – amygdaloid nuclei; subTHA - subthalamic region; VTA – ventral tegmental area; DR - dorsal raphe; and Tg – tegmental area. **(B)** Schematic diagram of the changes in ChIs projections in the mouse model of depression: In the wild type mice accumbal ChIs receive glutamatergic projections from three areas, medial orbital PFC (purple), vHIP (teal), and central amygdaloid nucleus (maroon), that appear to be important for their tonic activity and non-depressive phenotype. In the mouse model of depression inputs from the ventral hippocampus are significantly reduced, and tonic activity of the ChIs is severely changed, resulting in a depressive phenotype.

direct inputs from vHIP to NAc were found by others (LeGates et al., 2018), and confirmed in this study. LeGates et al. uncovered that the strength of the ventral hippocampal input to dopaminergic receptor 1 medium spiny neurons weakens in chronic stress, and this is linked to changes in reward response (LeGates et al., 2018). The role of this circuitry in depressive-like phenotype was further supported by another report showing that glutamatergic transmission from vHIP to NAc medium spiny neurons is increased in mice susceptible to stress (Bagot et al., 2015). Moreover, this effect is specific to vHIP-NAc circuitry since the stimulation of either mPFC or amygdala afferents to the NAc led to resilience. Our study shows for the first time cell-specific direct glutamatergic input from the vHIP to the NAc ChIs. Furthermore, this glutamatergic projection appears to have a decisive role in regulating the activity of the NAc ChIs in the ChAT-p11 cKO mice, as we found a significant reduction in the number of projections from this region, while projections from PFC, amygdala, and dorsal raphe are not changed significantly. It has been proposed that the behavioral output of the NAc depends on the amount of glutamate released from the inputs coming from the PFC and amygdala (Britt et al., 2012). It is possible that a decreased number of inputs from the vHIP to NAc ChIs disrupts the balance of signals received from other major glutamatergic inputs, including prefrontal cortical areas, CeN, and parafascicular thalamic nucleus. This would suggest that glutamatergic input disbalance is a key circuitry mechanism of depressive-like phenotype in ChAT-p11 cKO mice (Fig. 5). In addition, septum, basal forebrain, and habenula are rich in cholinergic neurons that do not express p11 in ChAT-p11 cKO mice. It is known that the basal forebrain (Campbell and Lobo, 2023; Morais-Silva et al., 2023), septum (Li et al., 2023), and habenula (Cui et al., 2018) play a key role in regulating depressive-like phenotype in mice. In this context, the absence of p11 in the ChIs in these regions and their inputs to NAc may also affect the physiology of the NAc ChIs and the behavioral phenotype related to depression. This cell-specific deletion of p11 and its mechanism of action in modulating the behavior, especially depressive- and anxiety-like phenotypes remains to be examined.

One fascinating outcome outside of the scope of this study is that p11 ablation in ChIs affects specifically the ChAT-vHIP circuitry but not others examined in this study. One possibility is that p11 affects the development of ChIs in a way that prevents the formation of inputs from the vHIP. Genetic ablation impact on ChAT circuitry development has been shown before, where the TrkA ablation impairs the basal forebrain-vHIP ChAT circuitry, specifically its laminar pattern and the number of projections (Sanchez-Ortiz et al., 2012). In rodents, ChIs development is tightly regulated by the NGF and BDNF signaling cascades trough their receptors, p75, TrkA, and TrkB, where the NGF/p75 determines the number of striatal ChIs (Ward and Hagg, 1999; Sanchez-Ortiz et al., 2012), while the BDNF/TrkB regulate growth and complexity of neurons, including loss of dendritic spines, and diminished nigral–striatal projections (Li et al., 2012). The mechanism by which p11 affects ChIs development may rely on a complex cascade involving plasmin, BDNF, NGF, and Anxa2, an important binding partner of p11. Results from the in vitro studies support this hypothesis. For example, it has been shown that NGF-induced neuritogenesis depends on the Anxa2-mediated plasmin generation (Jacovina et al., 2001), while p11 has been shown to be necessary for the BDNF-mediated effect on dendritic length and spine density (Park et al., 2016). However, the exact mechanism of p11-

induced changes in NAc ChIs circuitry shown here remains to be elucidated.

Limitations of the study related to the methodology

The difficulty of labeling sparse populations and areas deep within the brain, such as NAc, has so far prevented the mapping of the interneuronal subtypes in NAc. The optimal infection of scant populations, such as ChIs, requires a larger number of viral particles and a higher volume for injection, which then brings a risk of off-target infections in adjacent areas with the same type of cell. For example, olfactory bulb granule cells as well as olfactory tubercle neurons were very often labeled due to the infection of olfactory tubercle neurons and piriform cortex. To circumvent this constraint, various volumes of rabies viral particles were injected. While labeled cells were detected in the same areas of the brain, a much smaller number of cells was observed with a smaller volume. Thus, smaller volumes ensured the proper regional quantification, but the optimal visualization of the projection sites in the whole brain tissue had to be performed with a higher volume. Furthermore, in this study, even the smaller volume of the virus injected prevented us to discern between the projections to the core and shell of the NAc as the virus infected both areas of the NAc. We also detected some areas, particularly in the regions further away from the injection site, such as locus coeruleus or medulla, with the number of projections in single digits. This implied that the number of viral particles defined by the titer of the virus and the volume injected is very important for its propagation and consequently a number of labeled cells and quality of labeling, as suggested previously (Wall et al., 2013). Therefore, while this study used the approach in experimental design and rigorous analysis of virally labeled projection neurons, previously designed by others (Haubensak et al., 2010; Guo et al., 2015; Klug et al., 2018), these circuitries will need further confirmation by other methods, such as electrophysiology. In addition, the mouse line that used BAC-generated ChAT-CRE has been shown to overexpress the vesicular acetylcholine transporter, but this primarily has a downstream effect due to the excess acetylcholine and less effect on ChIs themselves (Crittenden et al., 2014; Straub et al., 2014). Thus, we believe that our study utilizing this transgenic mouse line closely represents this circuitry in wild type mice.

In summary, given the key role of the ChIs, and especially NAc ChIs in mood disorders, we elucidated the connectivity of the accumbal ChIs on the level of the whole brain and examined this connectivity in the context of the mouse model of depression. Specific behavioral patterns and clinical symptoms of depression depend on the correlations between specific networks between multiple brain areas, their interactions, and cell-specific circuits between these regions. In this context, the functional significance of our data warrants further mechanistic studies that will elucidate the role of the inputs to NAc ChIs from various brain regions and how they govern reward behavior and dysfunction in mood disorders. Furthermore, this study may further our understanding of the functional changes in the patients suffering from neurodegenerative diseases, such as Alzheimer's, Parkinson's, and Huntington's, which all have disrupted acetylcholine signaling in the striatum and often exhibit psychiatric symptoms.

Data availability

Data underlying this study are available in the published article.

Acknowledgments

Jeanne M. Nerbonne served as editor.

We thank Dr. Nathaniel Heintz for a generous gift of the ChAT-CRE and ChAT-TRAP mice lines (project Gene Expression Nervous System Atlas (GENSAT) Project, National Institute of Neurological Disorders and Stroke contracts N01NS02331 & HHSN271200723701C to The Rockefeller University). We are grateful to Dr. Urlich Muller (John Hopkins School of Medicine, Baltimore, MD, USA) for the Cux2-CRE mouse line. We thank Dr. Katia Manova-Todorova, the head of MSKCC Molecular Imaging Core Facility, Dr. Jerry Chang, and Dr. Thomas Liebman for help with the imaging, Mahira Tiwana for technical help with the experiments, Drs. Inez Ibanez-Tallon, Luca Parolari, and Jennifer Warner-Schmidt for helpful suggestions during this study, and Dr. Marc Flajolet who read the manuscript and offered thoughtful suggestions. We extend special thanks to Dina Becaj, a participant in the Rockefeller University Summer Science Research Program, who helped with the cell quantification experiments.

This work was supported by the Fisher Center for Alzheimer's Research Foundation (to P. Greengard), National Institute on Drug Abuse P30 DA035756 Pilot Project Award and National Institute on Aging 1RF1AG059770-01 (to A. Milosevic).

Author contributions: L. Medrihan: Conceptualization, Investigation, Validation, Visualization, Writing - original draft, Writing - review & editing, M.G. Knudsen: Data curation, Investigation, Writing - review & editing, T. Ferraro: Data curation, Validation, Writing - review & editing, P. Del Cioppo Vasques: Formal analysis, Investigation, Validation, Y. Romin: Formal analysis, Resources, S. Fujisawa: Data curation, Formal analysis, P. Greengard: Conceptualization, Funding acquisition, A. Milosevic: Conceptualization, Data curation, Formal analysis, Funding acquisition, Investigation, Methodology, Project administration, Resources, Supervision, Validation, Visualization, Writing - original draft, Writing - review & editing.

Disclosures: The authors declare no competing interests exist.

Submitted: 11 October 2024
Revised: 11 December 2024
Accepted: 6 February 2025

References

Alexander, B., J. Warner-Schmidt, T. Eriksson, C. Tamminga, M. Arango-Lievano, S. Ghose, M. Vernov, M. Stavarache, S. Musatov, M. Flajolet, et al. 2010. Reversal of depressed behaviors in mice by p11 gene therapy in the nucleus accumbens. *Sci. Transl. Med.* 2:54ra76. https://doi.org/10.1126/scitranslmed.3001079

Bagot, R.C., E.M. Parise, C.J. Peña, H.X. Zhang, I. Maze, D. Chaudhury, B. Persaud, R. Cachope, C.A. Bolaños-Guzmán, J.F. Cheer, et al. 2015. Ventral hippocampal afferents to the nucleus accumbens regulate

susceptibility to depression. *Nat. Commun.* 6:7062. https://doi.org/10.1038/ncomms8062

Basu, K., C. Gravel, R. Tomioka, T. Kaneko, N. Tamamaki, and A. Sík. 2008. Novel strategy to selectively label excitatory and inhibitory neurons in the cerebral cortex of mice. *J. Neurosci. Methods*. 170:212–219. https://doi.org/10.1016/j.jneumeth.2008.01.016

Berton, O., C.A. McClung, R.J. Dileone, V. Krishnan, W. Renthal, S.J. Russo, D. Graham, N.M. Tsankova, C.A. Bolanos, M. Rios, et al. 2006. Essential role of BDNF in the mesolimbic dopamine pathway in social defeat stress. *Science*. 311:864–868. https://doi.org/10.1126/science.1120972

Bolam, J.P., J.J. Hanley, P.A. Booth, and M.D. Bevan. 2000. Synaptic organisation of the basal ganglia. *J. Anat.* 196:527–542. https://doi.org/10.1046/j.1469-7580.2000.19640527.x

Britt, J.P., F. Benaliouad, R.A. McDevitt, G.D. Stuber, R.A. Wise, and A. Bonci. 2012. Synaptic and behavioral profile of multiple glutamatergic inputs to the nucleus accumbens. *Neuron*. 76:790–803. https://doi.org/10.1016/j.neuron.2012.09.040

Brown, M.T., K.R. Tan, E.C. O'Connor, I. Nikonenko, D. Muller, and C. Lüscher. 2012. Ventral tegmental area GABA projections pause accumbal cholinergic interneurons to enhance associative learning. *Nature*. 492:452–456. https://doi.org/10.1038/nature11657

Cachope, R., Y. Mateo, B.N. Mathur, J. Irving, H.L. Wang, M. Morales, D.M. Lovinger, and J.F. Cheer. 2012. Selective activation of cholinergic interneurons enhances accumbal phasic dopamine release: Setting the tone for reward processing. *Cell Rep.* 2:33–41. https://doi.org/10.1016/j.celrep.2012.05.011

Campbell, R.R., and M.K. Lobo. 2023. Pallidal circuits drive addiction behavior. *Trends Neurosci.*:S0166-2236(23)00228-X. https://doi.org/10.1016/j.tins.2023.10.001

Chaudhury, D., H. Liu, and M.H. Han. 2015. Neuronal correlates of depression. *Cell. Mol. Life Sci.* 72:4825–4848. https://doi.org/10.1007/s00018-015-2044-6

Chaudhury, D., J.J. Walsh, A.K. Friedman, B. Juarez, S.M. Ku, J.W. Koo, D. Ferguson, H.C. Tsai, L. Pomeranz, D.J. Christoffel, et al. 2013. Rapid regulation of depression-related behaviours by control of midbrain dopamine neurons. *Nature*. 493:532–536. https://doi.org/10.1038/nature11713

Cheng, J., G. Umschweif, J. Leung, Y. Sagi, and P. Greengard. 2019. HCN2 channels in cholinergic interneurons of nucleus accumbens shell regulate depressive behaviors. *Neuron*. 101:662–672.e5. https://doi.org/10.1016/j.neuron.2018.12.018

Christoffel, D.J., S.A. Golden, J.J. Walsh, K.G. Guise, M. Heshmati, A.K. Friedman, A. Dey, M. Smith, N. Rebusi, M. Pfau, et al. 2015. Excitatory transmission at thalamo-striatal synapses mediates susceptibility to social stress. *Nat. Neurosci.* 18:962–964. https://doi.org/10.1038/nn.4034

Collins, A.L., T.J. Aitken, I.W. Huang, C. Shieh, V.Y. Greenfield, H.G. Monbouquette, S.B. Ostlund, and K.M. Wassum. 2019. Nucleus accumbens cholinergic interneurons oppose cue-motivated behavior. *Biol. Psychiatry*. 86:388–396. https://doi.org/10.1016/j.biopsych.2019.02.014

Crittenden, J.R., C.J. Lacey, T. Lee, H.A. Bowden, and A.M. Graybiel. 2014. Severe drug-induced repetitive behaviors and striatal overexpression of VAChT in ChAT-ChR2-EYFP BAC transgenic mice. *Front. Neural Circuits*. 8:57. https://doi.org/10.3389/fncir.2014.00057

Cui, Y., Y. Yang, Z. Ni, Y. Dong, G. Cai, A. Foncelle, S. Ma, K. Sang, S. Tang, Y. Li, et al. 2018. Astroglial Kir4.1 in the lateral habenula drives neuronal bursts in depression. *Nature*. 554:323–327. https://doi.org/10.1038/nature25752

Doyle, J.P., J.D. Dougherty, M. Heiman, E.F. Schmidt, T.R. Stevens, G. Ma, S. Bupp, P. Shrestha, R.D. Shah, M.L. Doughty, et al. 2008. Application of a translational profiling approach for the comparative analysis of CNS cell types. *Cell*. 135:749–762. https://doi.org/10.1016/j.cell.2008.10.029

Epstein, J., H. Pan, J.H. Kocsis, Y. Yang, T. Butler, J. Chusid, H. Hochberg, J. Murrough, E. Strohmayer, E. Stern, and D.A. Silbersweig. 2006. Lack of ventral striatal response to positive stimuli in depressed versus normal subjects. *Am. J. Psychiatry*. 163:1784–1790. https://doi.org/10.1176/ajp.2006.163.10.1784

Franco, S.J., C. Gil-Sanz, I. Martinez-Garay, A. Espinosa, S.R. Harkins-Perry, C. Ramos, and U. Müller. 2012. Fate-restricted neural progenitors in the mammalian cerebral cortex. *Science*. 337:746–749. https://doi.org/10.1126/science.1223616

Franklin, K.B.J., and G. Paxinos. 2008. The Mouse Brain in Stereotaxic Coordinates, Compact. Third edition. Academic Press-Elsevier, New York, NY, USA.

Gerfen, C.R., and P.E. Sawchenko. 1984. An anterograde neuroanatomical tracing method that shows the detailed morphology of neurons, their axons and terminals: Immunohistochemical localization of an axonally transported plant lectin, Phaseolus vulgaris leucoagglutinin (PHA-L). *Brain Res.* 290:219–238. https://doi.org/10.1016/0006-8993(84)90940-5

Guo, Q., D. Wang, X. He, Q. Feng, R. Lin, F. Xu, L. Fu, and M. Luo. 2015. Whole-brain mapping of inputs to projection neurons and cholinergic interneurons in the dorsal striatum. *PLoS One*. 10:e0123381. https://doi.org/10.1371/journal.pone.0123381

Hanada, Y., Y. Kawahara, Y.N. Ohnishi, T. Shuto, M. Kuroiwa, N. Sotogaku, P. Greengard, Y. Sagi, and A. Nishi. 2018. p11 in cholinergic interneurons of the nucleus accumbens is essential for dopamine responses to rewarding stimuli. *eNeuro*. 5:ENEURO.0332-18.2018. https://doi.org/10.1523/ENEURO.0332-18.2018

Haubensak, W., P.S. Kunwar, H. Cai, S. Ciocchi, N.R. Wall, R. Ponnusamy, J. Biag, H.W. Dong, K. Deisseroth, E.M. Callaway, et al. 2010. Genetic dissection of an amygdala microcircuit that gates conditioned fear. *Nature*. 468:270–276. https://doi.org/10.1038/nature09553

Hultman, R., K. Ulrich, B.D. Sachs, C. Blount, D.E. Carlson, N. Ndubuizu, R.C. Bagot, E.M. Parise, M.T. Vu, N.M. Gallagher, et al. 2018. Brain-wide electrical spatiotemporal dynamics encode depression vulnerability. *Cell*. 173:166–180.e14. https://doi.org/10.1016/j.cell.2018.02.012

Jacovina, A.T., F. Zhong, E. Khazanova, E. Lev, A.B. Deora, and K.A. Hajjar. 2001. Neuritogenesis and the nerve growth factor-induced differentiation of PC-12 cells requires annexin II-mediated plasmin generation. *J. Biol. Chem.* 276:49350–49358. https://doi.org/10.1074/jbc.M106289200

Klug, J.R., M.D. Engelhardt, C.N. Cadman, H. Li, J.B. Smith, S. Ayala, E.W. Williams, H. Hoffman, and X. Jin. 2018. Differential inputs to striatal cholinergic and parvalbumin interneurons imply functional distinctions. *Elife*. 7:e35657. https://doi.org/10.7554/eLife.35657

LeGates, T.A., M.D. Kvarta, J.R. Tooley, T.C. Francis, M.K. Lobo, M.C. Creed, and S.M. Thompson. 2018. Reward behaviour is regulated by the strength of hippocampus-nucleus accumbens synapses. *Nature*. 564:258–262. https://doi.org/10.1038/s41586-018-0740-8

Li, L., R. Durand-de Cuttoli, A.V. Aubry, C.J. Burnett, F. Cathomas, L.F. Parise, K.L. Chan, C. Morel, C. Yuan, Y. Shimo, et al. 2023. Social trauma engages lateral septum circuitry to occlude social reward. *Nature*. 613:696–703. https://doi.org/10.1038/s41586-022-05484-5

Li, Y., D. Yui, B.W. Luikart, R.M. McKay, Y. Li, J.L. Rubenstein, and L.F. Parada. 2012. Conditional ablation of brain-derived neurotrophic factor-TrkB signaling impairs striatal neuron development. *Proc. Natl. Acad. Sci. USA*. 109:15491–15496. https://doi.org/10.1073/pnas.1212899109

Meredith, G.E., B.A. Baldo, M.E. Andrezjewski, and A.E. Kelley. 2008. The structural basis for mapping behavior onto the ventral striatum and its subdivisions. *Brain Struct. Funct.* 213:17–27. https://doi.org/10.1007/s00429-008-0175-3

Milosevic, A., T. Liebmann, M. Knudsen, N. Schintu, P. Svenningsson, and P. Greengard. 2017. Cell- and region-specific expression of depression-related protein p11 (S100a10) in the brain. *J. Comp. Neurol.* 525:955–975. https://doi.org/10.1002/cne.24113

Morais-Silva, G., R.R. Campbell, H. Nam, M. Basu, M. Pagliusi, M.E. Fox, C.S. Chan, S.D. Iñiguez, S. Ament, N. Cramer, et al. 2023. Molecular, circuit, and stress response characterization of ventral pallidum Npas1-Neurons. *J. Neurosci.* 43:405–418. https://doi.org/10.1523/JNEUROSCI.0971-22.2022

Muir, J., Y.C. Tse, E.S. Iyer, J. Biris, V. Cvetkovska, J. Lopez, and R.C. Bagot. 2020. Ventral hippocampal afferents to nucleus accumbens encode both latent vulnerability and stress-induced susceptibility. *Biol. Psychiatry*. 88:843–854. https://doi.org/10.1016/j.biopsych.2020.05.021

Niu, J.G., S. Yokota, T. Tsumori, T. Oka, and Y. Yasui. 2012. Projections from the anterior basomedial and anterior cortical amygdaloid nuclei to melanin-concentrating hormone-containing neurons in the lateral hypothalamus of the rat. *Brain Res.* 1479:31–43. https://doi.org/10.1016/j.brainres.2012.08.011

O'Donnell, P., A. Lavín, L.W. Enquist, A.A. Grace, and J.P. Card. 1997. Interconnected parallel circuits between rat nucleus accumbens and thalamus revealed by retrograde transynaptic transport of pseudorabies virus. *J. Neurosci.* 17:2143–2167. https://doi.org/10.1523/JNEUROSCI.17-06-02143.1997

Park, S.W., H. Nhu, H.Y. Cho, M.K. Seo, C.H. Lee, N.N. Ly, C.M. Choi, B.J. Lee, G.M. Kim, W. Seol, et al. 2016. p11 mediates the BDNF-protective effects in dendritic outgrowth and spine formation in B27-deprived primary hippocampal cells. *J. Affect. Disord.* 196:1–10. https://doi.org/10.1016/j.jad.2016.02.010

Paré, D. 2003. Role of the basolateral amygdala in memory consolidation. *Prog. Neurobiol.* 70:409–420. https://doi.org/10.1016/S0301-0082(03)00104-7

Pinto, A., and S.R. Sesack. 2000. Limited collateralization of neurons in the rat prefrontal cortex that project to the nucleus accumbens. *Neuroscience*. 97:635–642. https://doi.org/10.1016/S0306-4522(00)00042-7

Price, J.L., and W.C. Drevets. 2010. Neurocircuitry of mood disorders. *Neuropsychopharmacology*. 35:192–216. https://doi.org/10.1038/npp.2009.104

Pérez, C.A., S.A. Stanley, R.W. Wysocki, J. Havranova, R. Ahrens-Nicklas, F. Onyimba, and J.M. Friedman. 2011. Molecular annotation of integrative feeding neural circuits. *Cell Metab.* 13:222–232. https://doi.org/10.1016/j.cmet.2010.12.013

Russo, S.J., and E.J. Nestler. 2013. The brain reward circuitry in mood disorders. *Nat. Rev. Neurosci.* 14:609–625. https://doi.org/10.1038/nrn3381

Rymar, V.V., R. Sasseville, K.C. Luk, and A.F. Sadikot. 2004. Neurogenesis and stereological morphometry of calretinin-immunoreactive GABAergic interneurons of the neostriatum. *J. Comp. Neurol.* 469:325–339. https://doi.org/10.1002/cne.11008

Sanchez-Ortiz, E., D. Yui, D. Song, Y. Li, J.L. Rubenstein, L.F. Reichardt, and L.F. Parada. 2012. TrkA gene ablation in basal forebrain results in dysfunction of the cholinergic circuitry. *J. Neurosci.* 32:4065–4079. https://doi.org/10.1523/JNEUROSCI.6314-11.2012

Schindelin, J., I. Arganda-Carreras, E. Frise, V. Kaynig, M. Longair, T. Pietzsch, S. Preibisch, C. Rueden, S. Saalfeld, B. Schmid, et al. 2012. Fiji: An open-source platform for biological-image analysis. *Nat. Methods*. 9:676–682. https://doi.org/10.1038/nmeth.2019

Schmidt, E.F., J.L. Warner-Schmidt, B.G. Otopalik, S.B. Pickett, P. Greengard, and N. Heintz. 2012. Identification of the cortical neurons that mediate antidepressant responses. *Cell*. 149:1152–1163. https://doi.org/10.1016/j.cell.2012.03.038

Sesack, S.R., and A.A. Grace. 2010. Cortico-basal ganglia reward network: Microcircuitry. *Neuropsychopharmacology*. 35:27–47. https://doi.org/10.1038/npp.2009.93

Shepherd, G.M. 2013. Corticostriatal connectivity and its role in disease. *Nat. Rev. Neurosci.* 14:278–291. https://doi.org/10.1038/nrn3469

Shrestha, P., A. Mousa, and N. Heintz. 2015. Layer 2/3 pyramidal cells in the medial prefrontal cortex moderate stress induced depressive behaviors. *Elife*. 4:e08752. https://doi.org/10.7554/eLife.08752

Smith, Y., D.V. Raju, J.F. Pare, and M. Sidibe. 2004. The thalamostriatal system: A highly specific network of the basal ganglia circuitry. *Trends Neurosci.* 27:520–527. https://doi.org/10.1016/j.tins.2004.07.004

Stanley, S., S. Pinto, J. Segal, C.A. Pérez, A. Viale, J. DeFalco, X. Cai, L.K. Heisler, and J.M. Friedman. 2010. Identification of neuronal subpopulations that project from hypothalamus to both liver and adipose tissue polysynaptically. *Proc. Natl. Acad. Sci. USA*. 107:7024–7029. https://doi.org/10.1073/pnas.1002790107

Straub, C., N.X. Tritsch, N.A. Hagan, C. Gu, and B.L. Sabatini. 2014. Multiphasic modulation of cholinergic interneurons by nigrostriatal afferents. *J. Neurosci.* 34:8557–8569. https://doi.org/10.1523/JNEUROSCI.0589-14.2014

Stuber, G.D., D.R. Sparta, A.M. Stamatakis, W.A. van Leeuwen, J.E. Hardjoprajitno, S. Cho, K.M. Tye, K.A. Kempadoo, F. Zhang, K. Deisseroth, and A. Bonci. 2011. Excitatory transmission from the amygdala to nucleus accumbens facilitates reward seeking. *Nature*. 475:377–380. https://doi.org/10.1038/nature10194

Svenningsson, P., K. Chergui, I. Rachleff, M. Flajolet, X. Zhang, M. El Yacoubi, J.M. Vaugeois, G.G. Nomikos, and P. Greengard. 2006. Alterations in 5-HT1B receptor function by p11 in depression-like states. *Science*. 311:77–80. https://doi.org/10.1126/science.1117571

Thompson, R.H., and L.W. Swanson. 2010. Hypothesis-driven structural connectivity analysis supports network over hierarchical model of brain architecture. *Proc. Natl. Acad. Sci. USA*. 107:15235–15239. https://doi.org/10.1073/pnas.1009112107

Tye, K.M., R. Prakash, S.Y. Kim, L.E. Fenno, L. Grosenick, H. Zarabi, K.R. Thompson, V. Gradinaru, C. Ramakrishnan, and K. Deisseroth. 2011. Amygdala circuitry mediating reversible and bidirectional control of anxiety. *Nature*. 471:358–362. https://doi.org/10.1038/nature09820

Ventura-Silva, A.P., A. Melo, A.C. Ferreira, M.M. Carvalho, F.L. Campos, N. Sousa, and J.M. Pêgo. 2013. Excitotoxic lesions in the central nucleus of the amygdala attenuate stress-induced anxiety behavior. *Front. Behav. Neurosci.* 7:32. https://doi.org/10.3389/fnbeh.2013.00032

Virk, M.S., Y. Sagi, L. Medrihan, J. Leung, M.G. Kaplitt, and P. Greengard. 2016. Opposing roles for serotonin in cholinergic neurons of the ventral and dorsal striatum. *Proc. Natl. Acad. Sci. USA*. 113:734–739. https://doi.org/10.1073/pnas.1524183113

Wall, N.R., M. De La Parra, E.M. Callaway, and A.C. Kreitzer. 2013. Differential innervation of direct- and indirect-pathway striatal projection neurons. *Neuron*. 79:347–360. https://doi.org/10.1016/j.neuron.2013.05.014

Wall, N.R., I.R. Wickersham, A. Cetin, M. De La Parra, and E.M. Callaway. 2010. Monosynaptic circuit tracing in vivo through Cre-dependent targeting and complementation of modified rabies virus. *Proc. Natl. Acad. Sci. USA*. 107:21848–21853. https://doi.org/10.1073/pnas.1011756107

Wang, X., C. Zhang, G. Szábo, and Q.Q. Sun. 2013. Distribution of CaMKIIα expression in the brain in vivo, studied by CaMKIIα-GFP mice. *Brain Res.* 1518:9–25. https://doi.org/10.1016/j.brainres.2013.04.042

Ward, N.L., and T. Hagg. 1999. p75(NGFR) and cholinergic neurons in the developing forebrain: a re-examination. *Brain Res. Dev. Brain Res.* 118:79–91. https://doi.org/10.1016/S0165-3806(99)00133-9

Warner-Schmidt, J.L., E.F. Schmidt, J.J. Marshall, A.J. Rubin, M. Arango-Lievano, M.G. Kaplitt, I. Ibañez-Tallon, N. Heintz, and P. Greengard. 2012. Cholinergic interneurons in the nucleus accumbens regulate depression-like behavior. *Proc. Natl. Acad. Sci. USA*. 109:11360–11365. https://doi.org/10.1073/pnas.1209293109

Waselus, M., J.P. Galvez, R.J. Valentino, and E.J. Van Bockstaele. 2006. Differential projections of dorsal raphe nucleus neurons to the lateral septum and striatum. *J. Chem. Neuroanat.* 31:233–242. https://doi.org/10.1016/j.jchemneu.2006.01.007

Watabe-Uchida, M., L. Zhu, S.K. Ogawa, A. Vamanrao, and N. Uchida. 2012. Whole-brain mapping of direct inputs to midbrain dopamine neurons. *Neuron*. 74:858–873. https://doi.org/10.1016/j.neuron.2012.03.017

Witten, I.B., S.C. Lin, M. Brodsky, R. Prakash, I. Diester, P. Anikeeva, V. Gradinaru, C. Ramakrishnan, and K. Deisseroth. 2010. Cholinergic interneurons control local circuit activity and cocaine conditioning. *Science*. 330:1677–1681. https://doi.org/10.1126/science.1193771

Yoshimura, Y., J.L. Dantzker, and E.M. Callaway. 2005. Excitatory cortical neurons form fine-scale functional networks. *Nature*. 433:868–873. https://doi.org/10.1038/nature03252

Zahm, D.S. 2000. An integrative neuroanatomical perspective on some subcortical substrates of adaptive responding with emphasis on the nucleus accumbens. *Neurosci. Biobehav. Rev.* 24:85–105. https://doi.org/10.1016/S0149-7634(99)00065-2

Zahm, D.S., and J.S. Brog. 1992. On the significance of subterritories in the "accumbens" part of the rat ventral striatum. *Neuroscience*. 50:751–767. https://doi.org/10.1016/0306-4522(92)90202-D

Zhang, L., T.P. Su, K. Choi, W. Maree, C.T. Li, M.Y. Chung, Y.S. Chen, Y.M. Bai, Y.H. Chou, J.L. Barker, et al. 2011. P11 (S100A10) as a potential biomarker of psychiatric patients at risk of suicide. *J. Psychiatr. Res.* 45:435–441. https://doi.org/10.1016/j.jpsychires.2010.08.012

Supplemental material

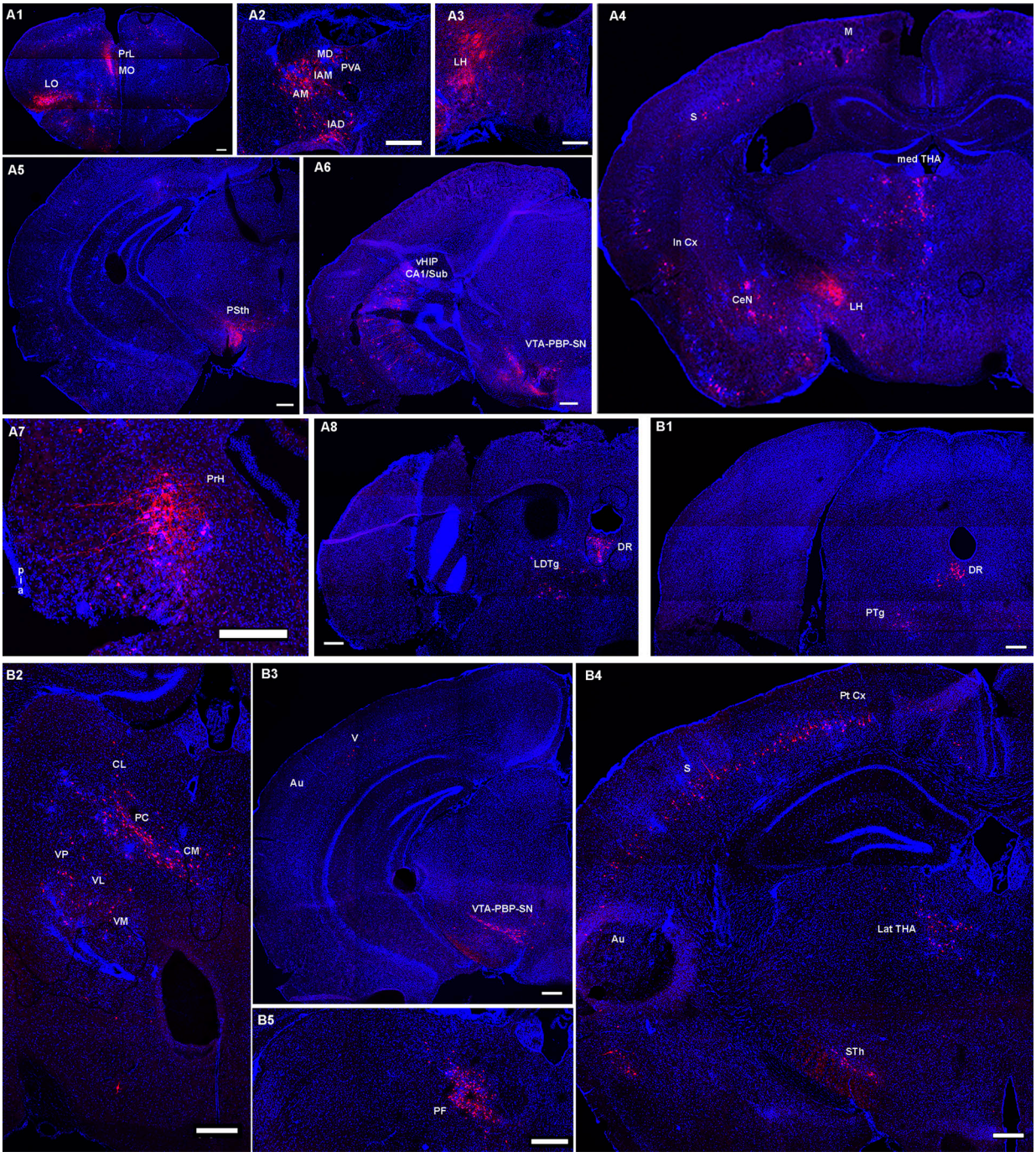

Figure S1. **Monosynaptic inputs to ChI cells in the ventral and dorsal striatum show regional differences.** Representative areas from the coronal sections of the brain injected into the NAc ChIs (A1–8) and CPu ChIs (B1–5) with the RV-mCherry. **(A1)** The whole brain section of the prefrontal cortex. **(A2)** Projecting neurons in thalamic nuclei PV, CM, MD, PC, IAD, IAM. **(A3)** Lateral hypothalamic area with a large number of projecting neurons. **(A4)** The whole brain section showing projecting neurons in the cortical areas M1 and 2, S1 and S2, insular cortical areas, central amygdaloid nuclei, ZI, and thalamic and hypothalamic nuclei. **(A5)** Area of the parasubthalamic nucleus contains projecting cells, while in the hippocampus small number of cells can be observed in the subiculum and CA1 area. **(A6)** In the more caudal area of the ventral hippocampus large number of labeled cells are found in the subiculum–CA1 regions. Cells are also visible in the VTA-PBP area. **(A7)** Perirhinal cortical area contains a large number of pyramidal neurons labeled with mCherry. **(A8)** Tegmental nuclei and dorsal raphe contain labeled cells in the lateral tegmental nuclei, and parabrachial nuclei. **(B1)** Labeled cells in the tegmental area that project to the CPu ChIs. Notice the absence of the labeled cells in the subiculum of the ventral hippocampus. **(B2 and B5)** Thalamic regions of the CPu-injected brain depicts different thalamic nuclei that project to the CPu ChIs. **(B3)** Substantia nigra, VTA-PBP-SN area contains a large number of cells labeled with the mCherry. Note the absence of labeled cells in the hippocampus. **(B4)** Whole brain image showing a large number of cortical areas that contain labeled cells, and strong labeling in the subthalamic and parasubthalamic nuclei. Scale bars in all images are 100 µm. Distance from the bregma: (A1) ~2.10 mm, (A2) approximately −0.82 mm, (A3) approximately −2.25 mm (A4) approximately −1.58 mm, (A5) approximately −2.60 mm, (A6) approximately −3.70 mm, (A7) approximately −1.94 mm, (A8) approximately −5.0 mm, (B1) approximately −4.36 mm, (B2) approximately −1.50 mm, (B3) approximately −3.10 mm, (B4) approximately −1.70 mm, (B5) approximately −2.10 mm.